

Reference Data: Spectra no DHQases

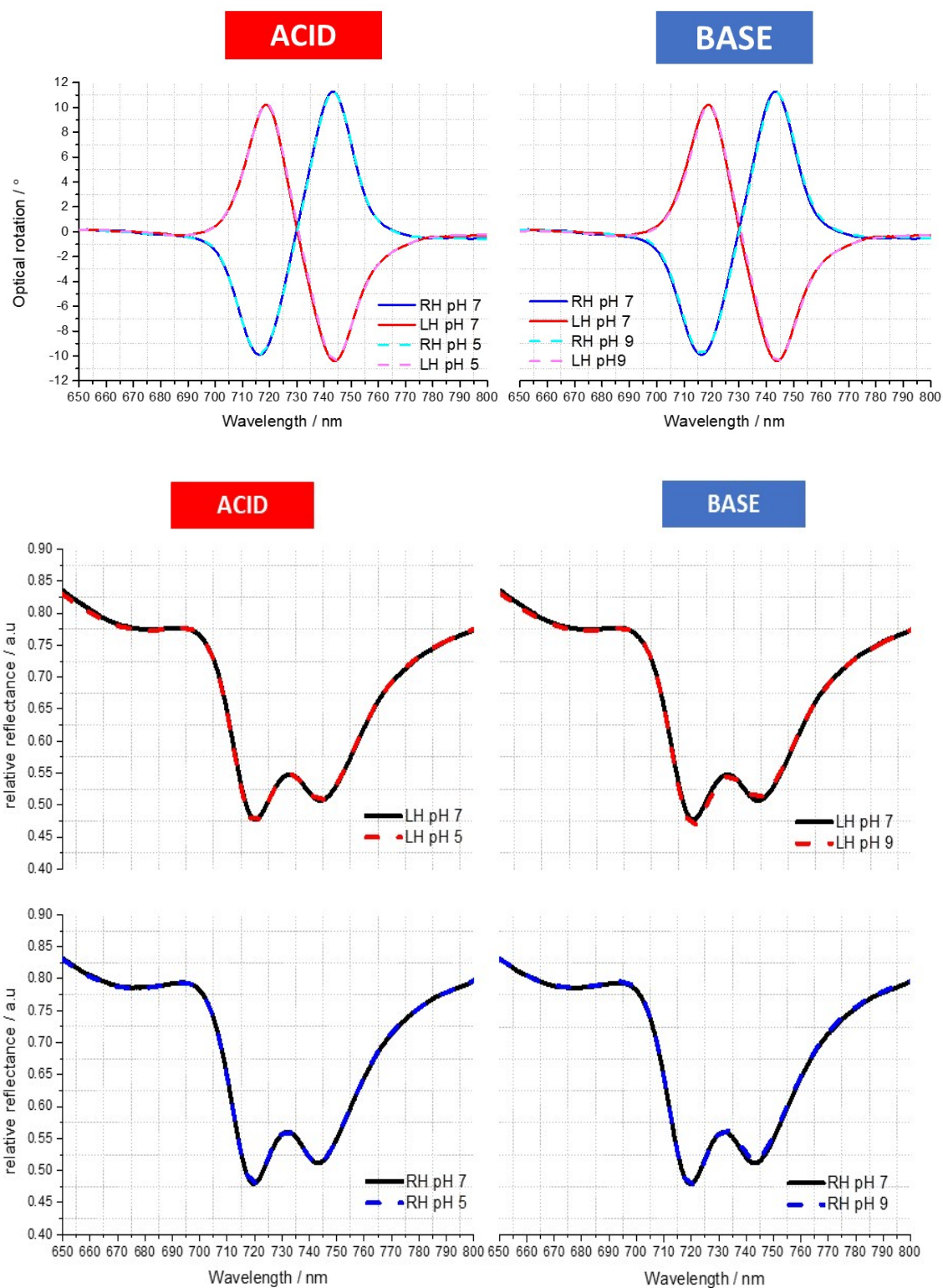


Figure S1: ORD (Upper Panels) and Reflectance (Lower Panels) spectra of LH and RH nanostructures from NTA coated substrate at pH 5, 7 and 9 without immobilised DHQases.

Phenomenological Model for fitting Reflectance Data.

The reflectance spectra displays a region of enhanced reflectivity. Such effects have been observed for this and other structures and are generically referred to as plasmonic induced reflectivity / transparency (PIR / PIT) depending on the measurements / substrate properties. These phenomena are considered classical all optical analogues of coherent quantum phenomena, electromagnetic induced transparency (EIT) and Autler-Townes splitting (ATS).³⁶ Although both effects give rise to transparency windows, they originate from different underlying physics. For EIT the transparency window arises from interference between different transition pathways. While for ATS splitting of levels due to high fields produce the transition window. Peng and co-workers have established criteria for assigning whether transparency in optical resonators originate from EIT or ATS analogues.²⁹

Consequently, factors derived from a simple classical model that replicates the PIR are used to parameterise protein induced asymmetries in the reflectance spectra. This model is based on two coupled oscillators, variations of this approach have been used in a number of studies to replicate PIR.³⁰ The starting point in this approach is a model system that is described by a set of two coupled harmonic helical oscillators:

$$\omega_r^{-2} \ddot{p}(t) + \gamma_r \omega_r^{-1} \dot{p}(t) + p(t) = g f(t) - \tilde{\kappa} q(t) \quad (1)$$

$$\omega_d^{-2} \ddot{q}(t) + \gamma_d \omega_d^{-1} \dot{q}(t) + q(t) = -\tilde{\kappa} p(t) \quad (2)$$

The radiative (bright) resonator is described by the excitation $p(t)$ with a resonance frequency ω_r and damping factor γ_r . Similarly, the dark mode excitation is described by $q(t)$ with a resonance frequency ω_d and damping factor γ_d . The two resonators are coupled via a coupling constant κ . The bright mode is driven by an external force $f(t)$ and g is a constant indicating the coupling strength between the oscillator and the external force. Unlike previous applications of the coupled oscillator model to plasmonic transparency, terms $e^{i\theta}$ and $e^{i\phi}$ are included, which account for retardation phase shifts, θ and ϕ , in the bright and dark mode excitations respectively. Both resonators are then coupled via a complex coupling coefficient $\tilde{\kappa} = \kappa e^{-i(\theta - \phi)}$. The solutions of (1) and (2) take the form:

$$p(t) = e^{-i\theta} P(\omega) e^{-i(\omega t)} \quad (3)$$

$$q(t) = e^{-i\phi} Q(\omega) e^{-i(\omega t)} \quad (4)$$

Assuming an effective medium approximation, and using the above equations, an expression for the reflectivity can be derived and used for fitting the experimental data. Consistent with previous studies we find that only ϕ shows significant changes, and it is this which is used to parameterise asymmetries.

Numerical EM Simulations

EM simulations were performed using a commercial finite-element package (COMSOL v4.4, Wave optics module). Periodic boundary conditions were used to emulate the array of nanostructures. Perfectly matched layer conditions were used above and below the input and output ports. Varying polarised EM wave was applied at normal incidence onto the structure. To overcome computational complexity we have modelled a solid shuriken structure on a polycarbonate substrate with the identical dimensions to the indentation of the metafilm. Thus the simulations are intended to provide a proof-of-concept, rather than an exact simulation of experimental results. To mimic the image charge chiral perturbation we have introduced a 10 nm thick domain on the top surface of the shuriken, which can be assigned a chiral asymmetry parameter (ξ) value. In Figure 1 S we display simulated ORD spectra for LH (red) and RH (blue) shurikens which have ξ values of $0+0i$ (solid) and $3\times 10^{-3} + 3\times 10^{-3}i$ (dashed). The LH and RH spectra for $\xi = 0$ are as expected mirror images of each other, and also exhibit a similar bisignate lineshape to those collected from the metafilm. The introduction of chiral layer breaks the mirror symmetry of the spectra. The asymmetry between the LH and RH spectra is parameterised by a $A = 0.95$, which is comparable to that observed in experiment.

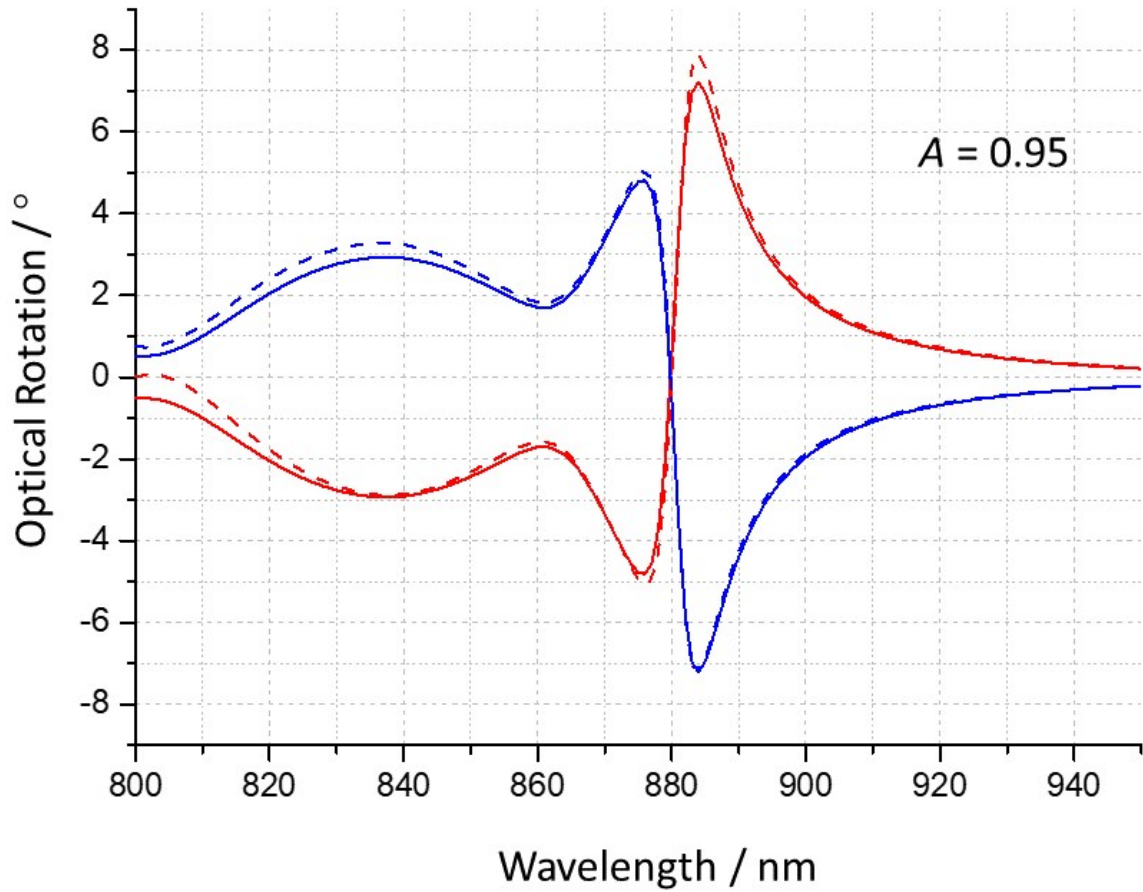


Figure S2. Simulated ORD spectra for LH (red) and RH (blue) shurikens which have ξ values of $0+0i$ (solid) and $3 \times 10^{-3} + 3 \times 10^{-3}i$ (dashed).

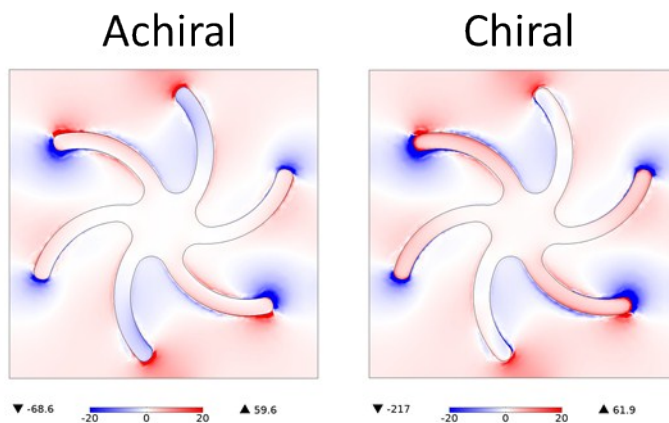


Figure S3. Optical chirality maps of generated for a LH structure. The introduction of the chiral layer increases the net LH chiral asymmetry of the near fields.

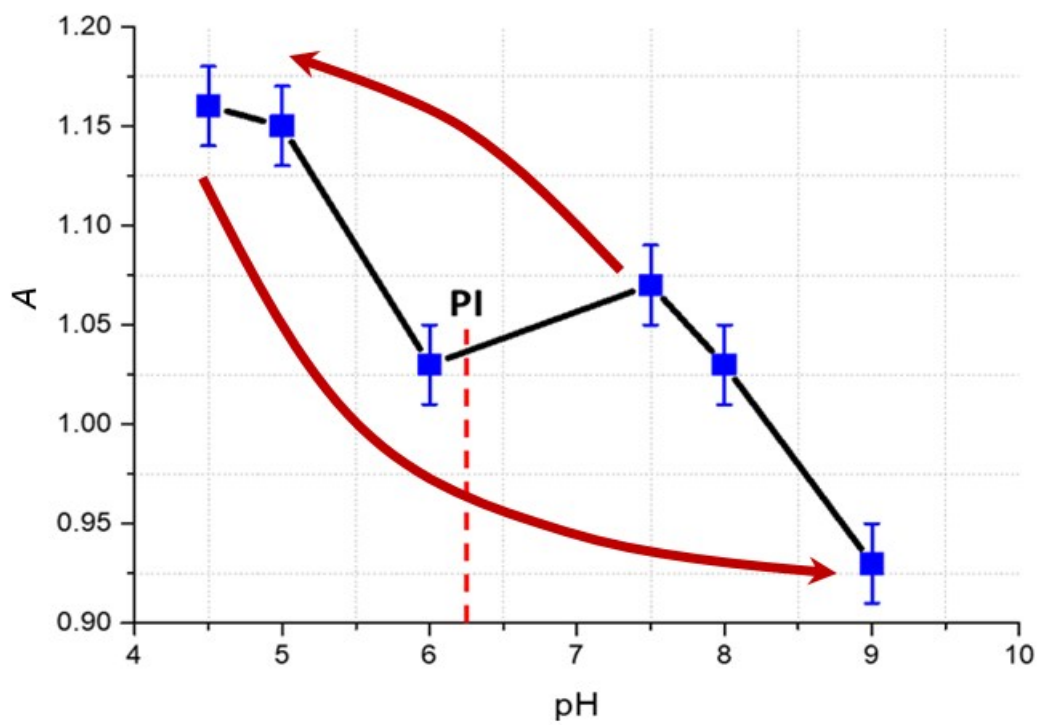


Figure S4. A pH titration curve of DHQ15. The red arrows illustrate the direction of change of pH. Measurements were collected in the following order of pH: 7.5, 6, 5, 4.5, 8 and then 9.

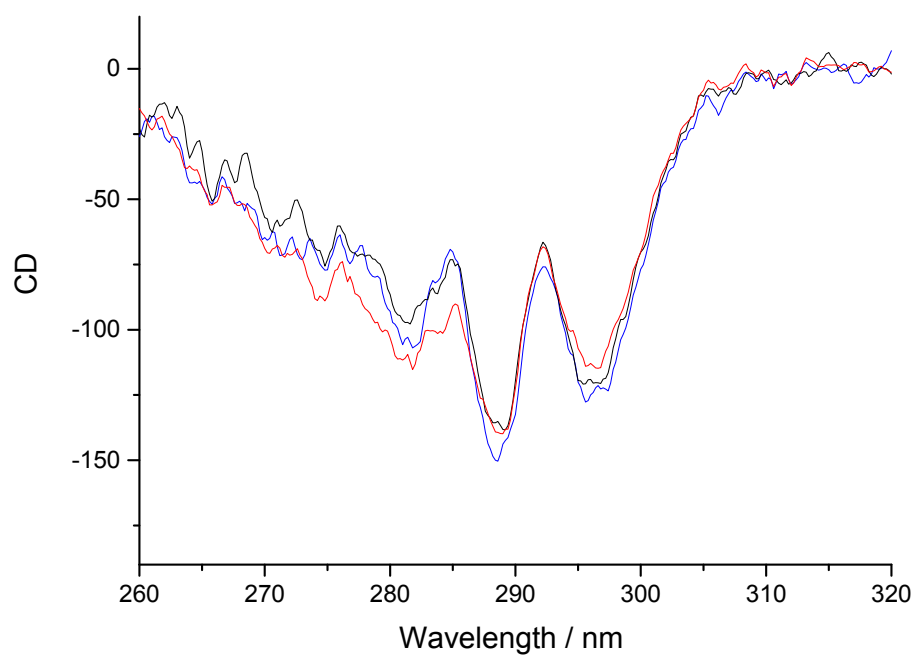


Figure S5. CD spectra of DHQ 15 taken in the near UV at three pHs: 5(red) , 7.5 (black) and 9 (blue).

fitting parameters ($\Delta\Delta x$)								
DHQ	5	12	15	27	28	33	36	38
ω_r	-0.50 \pm 0.20	0.00 \pm 0.20	-0.70 \pm 0.20	2.20 \pm 0.20	0.20 \pm 0.20	0.00 \pm 0.20	-1.90 \pm 0.20	-0.20 \pm 0.20
ω_d	-0.50 \pm 0.20	0.00 \pm 0.20	-1.00 \pm 0.20	2.20 \pm 0.20	0.20 \pm 0.20	0.00 \pm 0.20	-0.90 \pm 0.20	-0.20 \pm 0.20
κ	3.00 \pm $2.00 \cdot 10^{-04}$	-1.00 \pm $2.00 \cdot 10^{-04}$	-2.00 \pm $2.00 \cdot 10^{-04}$	5.00 \pm $2.00 \cdot 10^{-04}$	10.00 \pm $2.00 \cdot 10^{-04}$	-5.00 \pm $2.00 \cdot 10^{-04}$	-4.00 \pm $2.00 \cdot 10^{-04}$	2.00 \pm $2.00 \cdot 10^{-04}$
γ_r	0.00 \pm $3.00 \cdot 10^{-04}$	0.00 \pm $3.00 \cdot 10^{-04}$	4.00 \pm $3.00 \cdot 10^{-04}$	0.00 \pm $3.00 \cdot 10^{-04}$	-10.00 \pm $3.00 \cdot 10^{-04}$	0.00 \pm $3.00 \cdot 10^{-04}$	-1.50 \pm $3.00 \cdot 10^{-04}$	0.00 \pm $3.00 \cdot 10^{-04}$
γ_d	9.00 \pm $2.00 \cdot 10^{-04}$	5.00 \pm $2.00 \cdot 10^{-04}$	-5.00 \pm $2.00 \cdot 10^{-04}$	3.00 \pm $2.00 \cdot 10^{-04}$	10.00 \pm $2.00 \cdot 10^{-04}$	-4.00 \pm $2.00 \cdot 10^{-04}$	6.00 \pm $2.00 \cdot 10^{-04}$	6.00 \pm $2.00 \cdot 10^{-04}$
θ	0.00 \pm 0.20	0.00 \pm 0.20	0.00 \pm 0.20	0.00 \pm 0.20	0.00 \pm 0.20	0.00 \pm 0.20	0.00 \pm 0.20	0.00 \pm 0.20
ϕ	-0.60 \pm 0.20	-1.10 \pm 0.20	-2.90 \pm 0.20	0.00E+00 \pm 0.20	-2.00 \pm 0.20	0.90 \pm 0.20	2.30 \pm 0.20	-2.30 \pm 0.20

Table S1: fitting parameters extracted from the reflectance data for the representative DHQase proteins.

fitting parameters ($\Delta\Delta$)						
DHQ	15			38		
pH	5	7.5	9	5	7.5	9
ω_r	0.00 \pm 0.20	0.00 \pm 0.20	-0.20 \pm 0.20	0.55 \pm 0.20	1.05 \pm 0.20	0.80 \pm 0.20
ω_d	0.00 \pm 0.20	0.00 \pm 0.20	-0.20 \pm 0.20	0.50 \pm 0.20	1.00 \pm 0.20	0.80 \pm 0.20
κ	-11.5 \pm $2.00 \cdot 10^{-04}$	-14.00 \pm $2.00 \cdot 10^{-04}$	-38.5 \pm $2.00 \cdot 10^{-04}$	-3.00 \pm $2.00 \cdot 10^{-04}$	12.00 \pm $2.00 \cdot 10^{-04}$	4.5 \pm $2.00 \cdot 10^{-04}$
γ_r	-5.00 \pm $3.00 \cdot 10^{-04}$	0.00 \pm $3.00 \cdot 10^{-04}$	0.00 \pm $3.00 \cdot 10^{-04}$	-20.00 \pm $3.00 \cdot 10^{-04}$	0.00 \pm $3.00 \cdot 10^{-04}$	-20.00 \pm $3.00 \cdot 10^{-04}$
γ_d	-6.00 \pm $2.00 \cdot 10^{-04}$	-6.00 \pm $2.00 \cdot 10^{-04}$	-21.00 \pm $2.00 \cdot 10^{-04}$	1.00 \pm $2.00 \cdot 10^{-04}$	15.00 \pm $2.00 \cdot 10^{-04}$	12.00 \pm $2.00 \cdot 10^{-04}$
θ	0.00 \pm 0.20	0.00 \pm 0.20	0.00 \pm 0.20	0.00 \pm 0.20	0.00 \pm 0.20	0.00 \pm 0.20
ϕ	-1.50 \pm 0.20	-0.40 \pm 0.20	3.40 \pm 0.20	0.15 \pm 0.20	-2.30 \pm 0.20	-3.60 \pm 0.20

Table S2: fitting parameters extracted from the reflectance data for DHQ15 and DHQ38 at pH 5,7.5 and 9.

DHQase	5	12	15	27	28	33	36	38
5	1.00	0.493	0.420	0.425	0.469	0.521	0.893	0.527
12		1.00	0.441	0.451	0.476	0.596	0.473	0.466
15			1.00	0.418	0.430	0.448	0.413	0.435
27				1.00	0.541	0.476	0.411	0.493
28					1.00	0.479	0.469	0.483
33						1.00	0.528	0.525
36							1.00	0.507
38								1.00

Table S3: Pairwise sequence identity between different DHQase enzymes in this study, calculated using Jalview.³³

Table S4. Data collection, processing and refinement statistics for the enzymes DHQ15 and DHQ38.

Protein	DHQ15	DHQ38
Protein Data Bank accession code	6SME	6SMF
Space group	<i>P321</i>	<i>H3</i>
Unit cell <i>a, b, c</i> (Å)	128.65, 128.65, 75.72	133.61, 133.61, 101.63
Unit cell α, β, γ (°)	90.0, 90.0, 120.0	90.0, 90.0, 120.0
Data measured at beamline	I04-1 at Diamond Light Source, UK	I04-1 at Diamond Light Source, UK
Detector used	Pilatus 6M-F	Pilatus 6M-F
Wavelength (Å)	0.91587	0.91589
Resolution range (outer shell) ^a (Å)	75.72 - 1.65 (1.68 - 1.65)	66.90 - 2.34 (2.48 - 2.34)
Unique reflections	84,172 (4,397)	24,281 (1,215)
Redundancy	6.6 (6.6)	5.3 (5.5)
Completeness ellipsoidal (%)	97.0 (100.0)	94.0 (52.5) ^g
R_{merge}^b (%) / R_{pim}^b (%)	6.5 (150) / 2.7 (63.5)	4.5 (117) / 2.2 (55.6)
Mean I/σ	15.3 (1.3)	18.4 (1.4)
Refinement $R_{\text{work}} / R_{\text{free}}$ factors ^d (%)	15.2 / 17.4	16.4 / 21.2
Ramachandran plot features ^e (%)	96.4 / 3.6 / 0.0	93.7 / 6.2 / 0.2
Rms dev. bond lengths/angles (Å/°)	0.010 / 1.58	0.013 / 1.80
Coordinate error ^f (Å)	0.018 / 0.036	0.394 / 0.212
No. of non-H atoms used in refinement	4,822	4,526
No. of water molecules	346	91
Mean atomic/Wilson-plot B factors (Å ²)	31.3 / 25.1	91.0 / 74.8

^a Values in parentheses are for the highest-resolution outer shell.

^b $R_{\text{merge}} = \sum_{hkl} \sum_i |I_i(hkl) - \langle I(hkl) \rangle| / \sum_{hkl} \sum_i I_i(hkl)$, where \sum_i is taken over all observations of each reflection hkl and \sum_{hkl} is taken over all reflections hkl ;

$R_{\text{pim}} = \sum_{hkl} [1/(n_{hkl}-1)]^{1/2} \sum_i |I_i(hkl) - \langle I(hkl) \rangle| / \sum_{hkl} \sum_i I_i(hkl)$, where n_{hkl} is a number of all observations of reflection hkl .

^d R_{work} and $R_{\text{free}} = \sum_{hkl} | |F_o(hkl)| - |F_c(hkl)| | / \sum_{hkl} |F_o(hkl)|$; R_{work} was calculated for all data except for 5% that was used for the R_{free} calculations.

^e Percentages of residues in most favoured / additionally allowed / disallowed regions.

^f Estimated standard uncertainty; first value calculated using the method of Cruickshank, second one based on maximum likelihood as implemented in the CCP4 program REFMAC

^g The data showed significant anisotropy and only extended to 2.59 Å in the worst axis. Unobserved data have been removed but this has affected the completeness in the highest resolution shell even when considering elliptical completeness.

^e Percentages of residues in most favoured / additionally allowed / disallowed regions.

^f Estimated standard uncertainty; first value calculated using the method of Cruickshank, second one based on maximum likelihood as implemented in the CCP4 program REFMAC